Implantable wireless device for study of entrapment neuropathy

Ronit Malka[a,b,*], Diego L. Guarin[b], Suresh Mohan[b], Iván Coto Hernández[b], Pavel Gorelik[c], Ofer Mazor[c], Tessa Hadlock[b], Nate Jowett[b]

[a] Health Science and Technology Division, Harvard Medical School/Massachusetts Institute of Technology, Boston, MA, USA
[b] Surgical Photonics and Engineering Laboratory, Department of Otolaryngology – Head and Neck Surgery, Massachusetts Eye and Ear and Harvard Medical School, Boston, MA, USA
[c] Research Instrumentation Core, Department of Neurobiology, Harvard Medical School, Boston, MA, USA

GRAPHICAL ABSTRACT
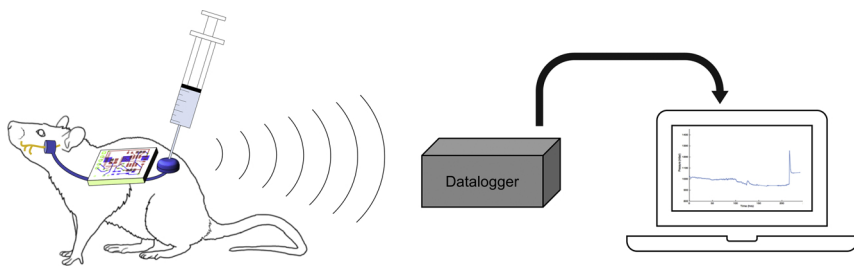
ARTICLE INFO

ABSTRACT

Background: Disease processes causing increased neural compartment pressure may induce transient or permanent neural dysfunction. Surgical decompression can prevent and reverse such nerve damage. Owing to insufficient evidence from controlled studies, the efficacy and optimal timing of decompression surgery remains poorly characterized for several entrapment syndromes.

New method: We describe the design, manufacture, and validation of a device for study of entrapment neuropathy in a small animal model. This device applies graded extrinsic pressure to a peripheral nerve and wirelessly transmits applied pressure levels in real-time. We implanted the device in rats applying low (under 100 mmHg), intermediate (200–300 mmHg) and high (above 300 mmHg) pressures to induce entrapment neuropathy of the facial nerve to mimic Bell's palsy. Facial nerve function was quantitatively assessed by tracking whisker displacements before, during, and after compression.

Results: At low pressure, no functional loss was observed. At intermediate pressure, partial functional loss developed with return of normal function several days after decompression. High pressure demonstrated complete functional loss with incomplete recovery following decompression. Histology demonstrated uninjured, Sunderland grade III, and Sunderland grade V injury in nerves exposed to low, medium, and high pressure, respectively.

Comparison with existing methods: Existing animal models of entrapment neuropathy are limited by inability to measure and titrate applied pressure over time.

Conclusions: Described is a miniaturized, wireless, fully implantable device for study of entrapment neuropathy in a murine model, which may be broadly employed to induce various degrees of neural dysfunction and functional recovery in live animal models.

1. Introduction

Entrapment neuropathies are vexing clinical conditions affecting over 40 million people worldwide yearly (Latinovic et al., 2006a). These conditions may yield chronic pain, numbness, muscle weakness, and spasticity (Gilden, 2004; Latinovic et al., 2006b). Many cranial and peripheral nerves and their roots are susceptible to entrapment, including those innervating regions of the head, neck, trunk, and extremities (Smith, 2014). The pathophysiology of dysfunction in entrapment neuropathy arises from increased pressure within a neural compartment secondary to intrinsic edema or extrinsic compression (Arnold and Elsheikh, 2013). Acute entrapment results in neural conduction block and focal demyelination; symptoms are fully reversible if neural compartment pressure normalizes before axonal degeneration occurs. With long-term compression and high compartment pressures, axonotmesis and Wallerian degeneration occur (Gaudet et al., 2011). Though peripheral and cranial nerve axons are capable of regeneration following axonotmesis, misdirection of extending axons to distal target tissues may occur, resulting in permanent neural dysfunction (Valls-Sole et al., 1992; Montserrat and Benito, 1988; Sumner, 1990; Weber and Newman, 2007; Teasdall and Salman, 1971; de Ruiter et al., 2008). Management of entrapment neuropathy may depend on several factors, including symptom severity and chronicity, results of electrophysiology studies, and patient co-morbidities. Surgical decompression of neural compartments has proven effective for management of several entrapment neuropathies, including carpal (Phalen and Kendrick, 1957) and cubital tunnel syndromes (Adelaar et al., 1984). However, the optimal timing of surgical decompression varies widely among different entrapment neuropathies, and is often not at the time of diagnosis but rather after more conservative medical management has failed or poor long-term functional prognosis has been established.

Bell's palsy (BP) is the most common acute cranial neuropathy. It is believed to result from entrapment of the facial nerve within its bony canal secondary to inflammatory edema following viral reactivation (Fisch and Esslen, 1972; Murakami et al., 1996). In two prospective surgical studies, Fisch and Gantz demonstrated clinically-significant improvement in long-term facial functional recovery among patients presenting with severe BP who underwent decompression surgery within two weeks of palsy onset (Fisch, 1981; Gantz et al., 1999). Though several subsequent studies have reported similar benefits of acute facial nerve decompression in the setting of severe BP (Liu et al., 2013; Shapira et al., 2006; Wu et al., 2015; Hato et al., 2012; Cannon et al., 2015; Bodenez et al., 2010), the procedure remains controversial (Smouha et al., 2011). Heretofore, clinical studies of facial nerve decompression have been limited by patient selection bias, inconsistent surgical technique, and suboptimal evaluation of long-term recovery. Due to its close proximity to the inner ear, surgical decompression of the facial nerve carries risk of permanent hearing loss. Owing to procedural risk and lack of evidence from prospective controlled studies to support its effectiveness, clinical practice guidelines remain neutral on facial nerve decompression for acute BP (Baugh et al., 2013). A controlled animal model of facial nerve decompression could inform clinical management of acute facial palsy.

Prior work has employed animal models for study of entrapment and related neuropathies, including Bell's palsy, carpal tunnel syndrome, spinal stenosis, sciatica, and diabetic neuropathy (Barac et al., 2013; Cheung et al., 2019; Aguayo et al., 1971; Gupta et al., 2004; Hazama et al., 1972) Entrapment of peripheral nerves in animal models has been induced using tourniquets, inflatable cuffs, spring-loaded clamps, implanted silicone tubing, and adhesive molds (Barac et al., 2013; Cheung et al., 2019; Aguayo et al., 1971; Gupta et al., 2004; Hazama et al., 1972; Rempel et al., 1999; Dellon and Mackinnon, 1991; Mackinnon et al., 1985; O'Brien et al., 1987; Liu et al., 2018; Chao et al., 2008; Aguayo et al., 1971; Dahlin and McLean, 1986; Dyck et al., 1990). However, precise pressure titration is an important feature that permits modeling of various degrees of severity of nerve entrapment, while continual measurement enables monitoring of pressure changes arising from biological responses to extrinsic compression, including demyelination, fluid shifts, and inflammatory cell migration. Thus, the study of nerve entrapment in animal models to date has been limited by the inability to measure and titrate applied pressure over the long term *in vivo*. Herein, we present the development and validation of an implantable device for controlled study of entrapment neuropathy. The device allows for graded extrinsic compression of surgically accessible nerves in small animals, concurrent with wireless monitoring of applied pressure for up to several months. Devices were implanted in live rats for compression of facial nerve branches to simulate BP. Facial nerve function was longitudinally assessed by quantification of whisking activity and correlated to applied pressure levels. After sacrifice, facial nerve sections were examined to evaluate for histological evidence of Wallerian degeneration and axonal regeneration.

2. Materials and methods

2.1. Design

We designed a biocompatible, sterilizable, and reusable implant that communicates wirelessly with an external receiver via radiofrequency. The devices wirelessly relay *in vivo* temperature and pressure data of an enclosed hydraulic system. Data may be stored in a datalogger for offline analysis or transmitted to a computer for online analysis (Fig. 1). The specifications of the implant and receiver design are described in greater detail in the supplementary material.

2.1.1. Implant

The implant consists of a microcontroller, wireless transmitter, pressure sensor, and battery integrated on a printed circuit board (PCB), connected to a fluid injection port and pressurizable cuff as shown in Fig. 2. In this example, the cuff is secured around a peripheral nerve. Pressure within the system is titrated by injection of liquid through a biocompatible injection port and is monitored by a pressure sensor. The entire assembly measures 25 mm x 20 mm x 15 mm and weighs under 15 g after biocompatible silicone embedding.
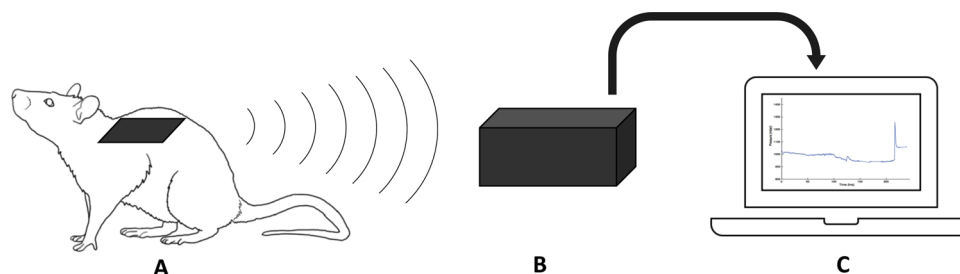

Fig. 1. Workflow diagram showing implanted device (A) wirelessly transmitting data collected in vivo to a datalogger (B), which then logs the data for further analysis (C).
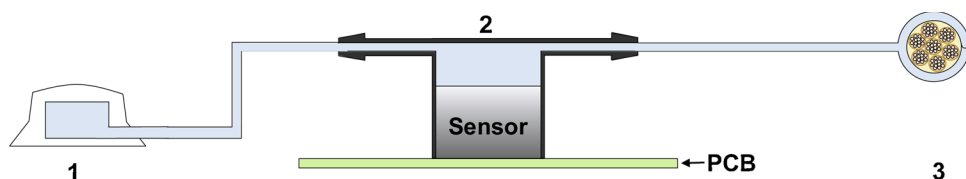
Fig. 2. Diagram of connections between implantable injection port (1), 3D printed fitting (2) PCB including integrated sensor (diagrammed), microcontroller, and battery (not shown), and occlusion cuff (3) surrounding nerve. Fluid (blue) can flow freely between the port, sensor, and cuff in this closed hydraulic system.

2.1.2. Pressure validation

As the device is required to hold and detect changes in pressure within the hydraulic system over time, validation of dynamic and static pressure measurements was performed. The precision of the device's sensor pressure measurement was quantified by comparing the difference in sensor measurements and analog pressure regulator readings when connected in parallel to compressed air. Dynamic pressure change was additionally evaluated by measuring the time the sensor measurements took to equilibrate to analog readings.

2.1.3. Receiver

A standalone external microcontroller acts as a datalogging receiver for data broadcasted by the implant. The receiver can be configured as a portable device that accompanies the animal's cage and stores data in an external drive for long-term experiments.

2.2. Fabrication

2.2.1. Printed circuit board

A customized PCB was created to minimize device footprint while integrating the microcontroller, sensor, and coin battery. The board was designed in free circuit board design software (EAGLE PCB Design Software, Autodesk Inc., San Rafael, CA) and printed using a commercial vendor (Sunstone Circuits, Mulino, OR). All hardware on the board were commercially available and reusable across multiple experiments. PCB design and component list are provided in the supplementary material.

2.2.2. Cuff and injection port

The occlusion cuff employed for nerve compression (Vascular Occlude Cuff, Access Technologies, Skokie, IL) was connected to the pressure sensor and a subcutaneous injection port (Rat-o-port, Access Technologies, Skokie, IL) using inelastic biocompatible hollow tubing to enable titration and monitoring of system pressure *in vivo*. A custom
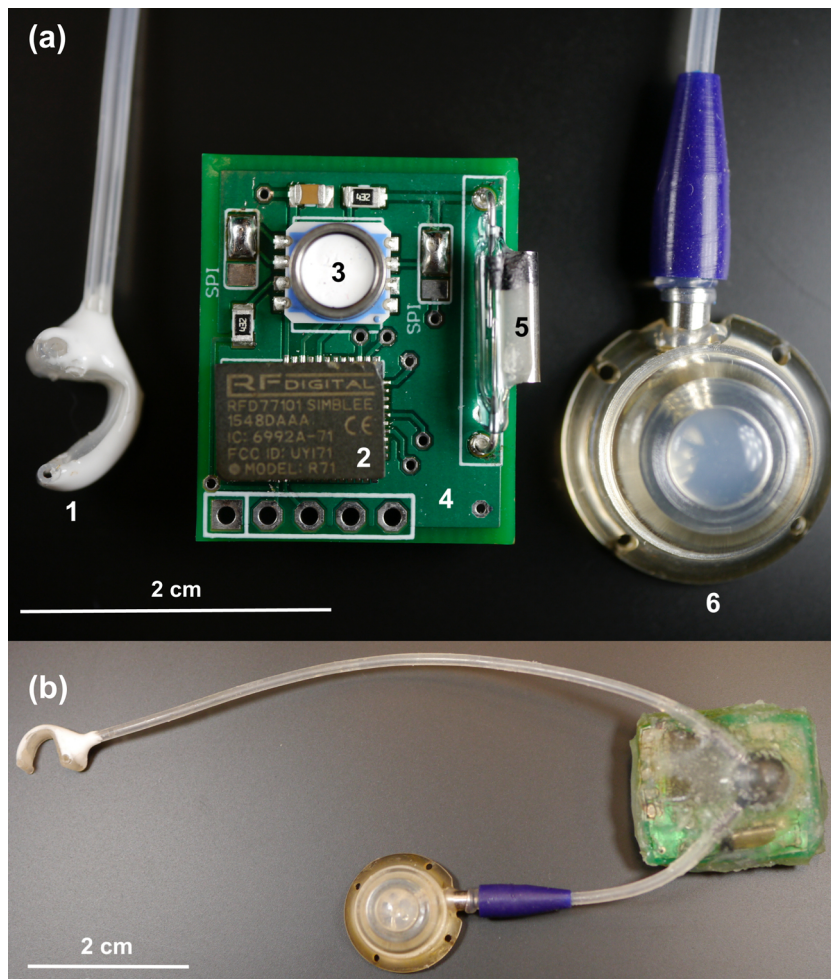

Fig. 3. (a) Implant deconstructed without silicone encasement, showing (1) hydraulic cuff, (2) microcontroller (Simblee), (3) pressure sensor, (4) printed circuit board, (5) magnetic switch, and (6) subcutaneous injection port. (b) Implant with parts assembled and encased in silicone. The coin cell battery is integrated onto the opposite side of the PCB (not shown).

coupler for connecting hydraulic system components was designed in SolidWorks (SolidWorks 3D CAD, Dassault Systémes, Waltham, MA) and 3D printed. Coupler design is available as supplementary material.

The occlusion cuff employed is air and water permeable, allowing for osmotic gradients following injection of non-permeable glycerol into the system to dictate pressure changes. The gradual shift of water into the system and resultant increase in hydrostatic pressure models that postulated to occur in entrapment neuropathies secondary to inflammation in a confined space (Rempel and Diao, 2004).

2.2.3. Silicone coating

The device body was coated in a thin layer of epoxy (Loctite QuickSet Epoxy, Loctite Industrial, Westlake, OH) to waterproof the board. It was then coated with 2 mm of medical-grade silicone (A-103 Medical Grade Elastomer, Factor II Inc., Lakeside, AZ) to protect the device from corrosion and render the implant biocompatible. A deconstructed diagram of the implant, as well as the final device, is shown in Fig. 3.

2.2.4. Sterilization

The silicone-coated device was sterilized with ethylene oxide (7 h at 46 °C) and degassed under vacuum for 5 days prior to implantation.

2.3. Surgical procedures

Experiments were performed in accordance with the National Institutes of Health Guide for the Care and Use of Laboratory Animals, with Institutional Animal Care and Use Committee approval.

2.3.1. Head fixation

Three female Lewis rats, aged 65–90 days, were anesthetized with isoflurane (3.5% during induction, 2% during operation) until unresponsive to toe-pinch. Meloxicam (1 mg/kg) and buprenorphine (0.1 mg/kg) were injected subcutaneously. A 2 cm incision was made midline over the calvarium, and bone cleared of overlying tissues. A percutaneous titanium head-fixation device was affixed to the calvarium using five titanium screws as previously described (Heaton et al., 2008) and the incision closed primarily using 5-0 polyglactin 910 suture (Vicryl Rapide, Ethicon US, LLC., Bridgewater, NJ). Topical bacitracin zinc antibiotic ointment was applied to the wound, and animals recovered from general anesthesia and returned to their cages. Meloxicam (1 mg/kg/day) was administered subcutaneously for 72 h postoperatively.

2.4. Behavioral conditioning and facial nerve functional testing

Two weeks following head fixation device implantation, animals underwent daily conditioning to restraint in a cloth sack until able to tolerate twenty minutes of continuous restraint without distress. Animals were then conditioned to head and body restraint for high-frame rate video capture of whisker movements. Facial nerve function was assessed by comparison of mean amplitude of whisking movements between sides. The design, setup, and signal processing underlying this functional assessment system is explained in greater detail in the supplementary section.

2.4.1. Implantation

Device hydraulic systems were filled with normal saline to neutral pressure (0 mmHg above atmospheric). Once conditioned, animals were again placed under isoflurane general anesthesia as above. After administration of analgesia, a 1.5 cm transverse incision was made in the left cheek, and skin-muscle flaps elevated atop the buccal and marginal mandibular branches of the left facial nerve (which carry motor efferents innervating the whisker pad musculature). The nerve branches were then circumferentially dissected in meticulous fashion without transection. Next, a 3 cm incision was made over the scapular portion of the dorsum, and a subcutaneous pocket created to receive the body of the device and injection port. The occlusion cuff with attached tubing was then tunneled subcutaneously between the dorsal and left facial incisions. The cuff was then secured around the dissected buccal and marginal mandibular branches with a 4-0 polypropylene suture (Fig. 4b). The device body and injection port were then secured to the fascia of the latissimus dorsi muscles using 5-0 absorbable polygalactin 910 sutures, and skin incisions closed in a single layer using identical suture (Fig. 4c). Animals were recovered from general anesthesia and perioperative care delivered as described above. Awake whisking function was documented by high-frame rate video capture immediately prior to surgery and again 3 days post-operatively to ensure no iatrogenic neural insult occurred secondary to device implant.

2.5. Modeling nerve entrapment

Three days following implantation, a 50% glycerol solution (0.01, 0.02 or 0.03 mL) was injected into device ports of the three animals. Injection volumes employed avoided pressure spikes; the colloid osmotic pressure of the injected glycerol induced gradual pressure rise by the movement of water across the semipermeable membranes of the occlusion cuffs. Additional small volumes (0.01 to 0.02 mL of 50%–90% glycerol solution) were again injected on post-operative day (POD) # 3 and 4 until gauge pressure ranges under 100 mmHg ('low-pressure'), between 200 and 300 mmHg ('medium-pressure'), and between 300 and 500 mmHg ('high-pressure') were achieved.

2.6. Device explant

Nerve decompression via device explant was planned after five days of compression for low, medium, and high-pressure groups. This duration is clinically relevant, as it falls within the 3–14 day window wherein facial nerve decompression is currently considered in humans with acute Bell's palsy. Decompression was achieved by removal of fluid from the injection ports, followed by immediate removal of the devices under general anesthesia to simulate decompression surgery. The occlusion cuff was meticulously freed from left facial nerve branches, and the device body and injection port with attached tubing extirpated through the dorsal incision. Incisions were closed in a single layer, and post-operative care delivered as described above. Whisker function was assessed daily for 7 days following decompression, followed by weekly assessment until a recovery plateau was noted for up to 12 weeks.

Fig. 4. *Device implantation:* (a) The occlusion cuff and device body with adjacent injection port are shown prior to securing to underlying tissues and wound closure. (b) The occlusion cuff is shown in position around the marginal and buccal branches of the facial nerve. (c) Animal 3 days post-operatively with implant body (anterior) and injection port (posterior) visible under the skin of the dorsum.

2.7. Nerve tissue processing

Upon study termination, animals were humanely euthanized in accordance with institutional animal care protocols. Corpses were immediately transcardially perfused with 4% phosphate-buffered paraformaldehyde (PFA). Left facial nerves were harvested and post-fixed by immersion in 4% PFA for 48 h, followed by cryoprotection in 30% sucrose for 24 h. Nerves were sharply divided into proximal, lesional (in the area of cuff compression), and distal segments. Axial cryosections at 1 μm were obtained and stained with FluoroMyelin® Green (1:300, Molecular Probes, Eugene, OR), similar to previously described methods (Wang et al., 2019; Mohan et al., 2018).

2.8. Tissue imaging

Fluorescent images of nerve cross-sections were collected with a confocal microscope (Leica Microsystems SP8, Wetzlar, Germany) equipped with a resonant scanner and 64X (1.3 NA) oil-immersion objective lens. FluoroMyelin® Green was excited with a 488 nm Argon laser, and fluorescent signal collected at 550/50 nm using Leica HyD hybrid detectors controlled with the Leica Application Suite X software. Proprietary deconvolution software (Lightning, Leica Microsystems) was uniformly employed for image enhancement. Image brightness and contrast were uniformly adjusted for enhanced visualization using ImageJ software (Fiji Distribution, Version 1.52e) (Schindelin et al., 2012; Schneider et al., 2012).

2.9. Image processing

High-powered fields (63X) were obtained for nerve histomorphometry. Mean myelinated axon count and diameter were quantified using a trainable random forest machine learning algorithm in commercial software (DRVISION Technologies, Bellevue, WA).

3. Results

3.1. Pressure validation

Fig. 5a demonstrates measurements obtained from analog and device sensors during rapid pressurization and depressurization. The implantable sensor captured rapid pressure changes and demonstrated near perfect agreement with analog gauge pressure within seconds. Fig. 5b and c demonstrate measurements obtained from analog and implantable sensors over a long-term measurement, with an initial injection pressure of 300 mmHg. The device maintained and wirelessly transmitted pressure measurements in close agreement with analog measurements (mean difference of 19 mmHg, SD, 6.9 mmHg) over six days.
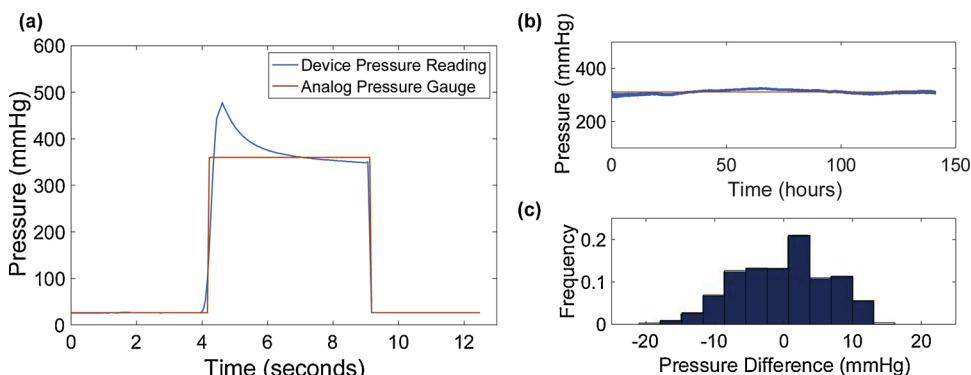
3.2. Device lifespan and implantation

Herein, devices were well tolerated during the eight day implantation with lossless data transmission prior to surgical explant (Fig. 4c). No signs of device extrusion occurred over the course of the study. As described in Supplementary Materials, in a second subset of animals, devices were well tolerated *in vivo* and provided continuous transmission of pressure and temperature readings once per hour for over 10 weeks using a 12 mm coin battery (Eunicell™ CR1220, 40 mA h, East Technology Co., Shenzen District, China). Use of a larger battery (Eunicell™ CR2032, 235 mA h, East Technology Co., Shenzen District, China) in the devices allowed for continuous operation of the devices for more than five months. These durations of neural compression are sufficient for modeling various nerve entrapment syndromes (Rempel et al., 1999; Rempel and Diao, 2004). Reuse of the devices is possible by careful removal of the silicone and resin coatings, replacement of the single-use battery, followed by recoating with resin and silicone and resterilization. Future designs will seek to incorporate rechargeable batteries paired with externalized waterproof pin connectors for *ex vivo* recharging of the devices, or the addition of inductive or resonant inductive wireless charging components for *in vivo* recharging.

3.3. Pressure threshold determination

As demonstrated in Fig. 6, low-pressure facial nerve compression (less than 100 mmHg) resulted in no detectable impairment in whisking function following 5 days of compression. Rapid and complete loss of whisking activity was noted for the rat whose facial nerve was compressed in the range of 300 mmHg–500 mmHg within 24 h; only partial recovery of whisking function was noted 12 weeks following decompression. Gradual and incomplete loss of whisking function occurred for the rat whose facial nerve was compressed between 200–300 mmHg over the course of 72 h; subsequent decompression resulted in complete recovery of normal whisking activity within 48 h.

3.4. Histology

At time of device removal, healthy appearing nerve was grossly noted within the cuff inflated to a low gauge pressure (under 100 mm Hg) (Fig. 7a), while some thinning and partial clarification was noted for facial nerve branches compressed at medium pressure (200 mmHg – 300 mmHg) (Fig. 7b-c). Nerve branches compressed between 300 mmHg and 500 mmHg demonstrated extreme thinning and discontinuity, believed secondary to ischemic necrosis from prolonged high-pressure compression.

Histologic evaluation of harvested facial nerves 12 weeks after nerve decompression and device explant demonstrated varying degrees of neural injury and regeneration, correlating with the level of applied pressure (Fig. 8). In nerve compressed at low-pressure, myelin thickness and axon caliber appeared normal across proximal, lesional, and distal segments. Nerve compressed at medium pressure demonstrated
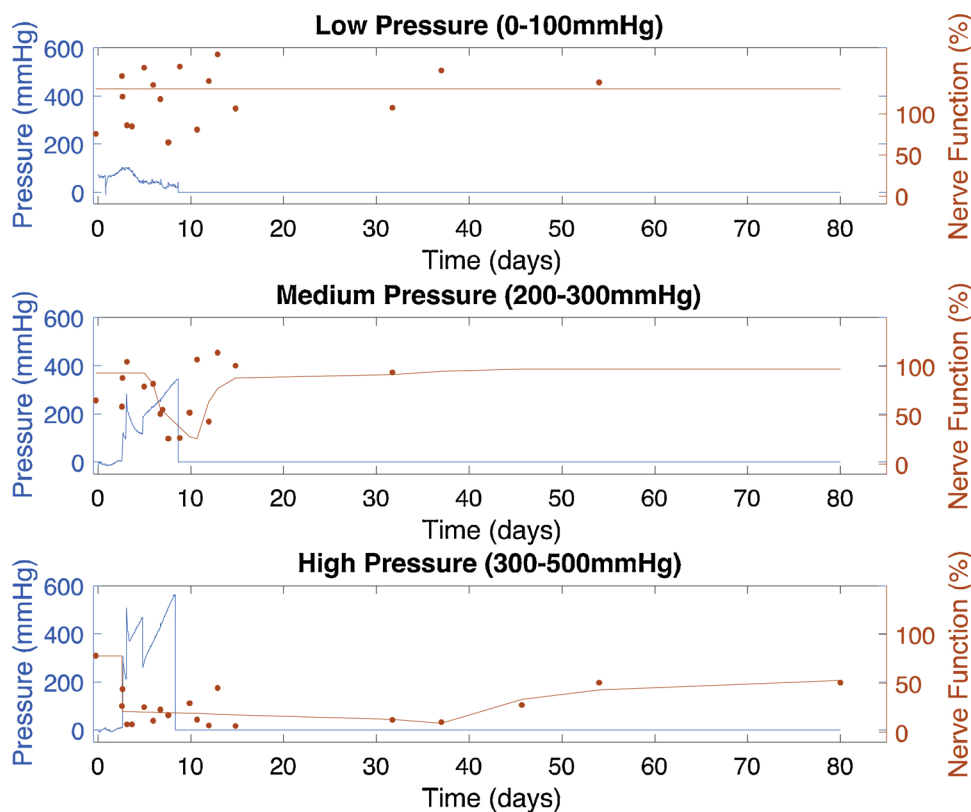

Fig. 5. *Pressure measurement validation using an analog pressure gauge attached to the device* (a) Simulation of rapid pressure change. Wireless device pressure (blue line, sampling rate of 500 Hz) and analog pressure (red line) measurements are shown for a single injection bolus. (b) Device pressure (sampling rate of 1/60 Hz) and analog pressure measurements (daily) over six days following a single injection bolus into the system; (c) histogram of differences between device and analog pressure readings over six days.

Fig. 6. *Comparison of nerve occlusion cuff pressure and whisking function for three different pressurization levels.* Shown in blue are device pressure readings (sampling rate of once per hour) for low (under 100 mmHg), medium (200–300 mmHg), and high (300–500 mmHg) pressurization targets. Shown in orange are nerve functional measurements, calculated as a percentage of awake behavioral whisking amplitude compared to the control (unoperated) side. At low compression pressure (under 100 mmHg), no functional whisking impairment is demonstrated. At high compression pressure, rapid and complete loss of whisking activity occurred, with incomplete recovery noted 12 weeks following nerve decompression. At medium compression pressure, gradual and incomplete loss of whisking activity is noted, with complete recovery of function noted within 2 days of decompression.

sporadic axonotmesis and occasional endoneurial disruption, suggestive of a Sunderland grade III neural injury (Sunderland, 1951). As demonstrated in Fig. 8, partial axonotmesis was evidenced by occasional Wallerian degeneration in lesional segments and the putative presence of 'regenerating units' in the distal segment of nerve compressed at medium pressure. Regenerating units comprise multiple tightly-spaced small-diameter and thinly-myelinated 'daughter' axons, which sprout from a single large myelinated axon following axotomy (Morris et al., 1972). Regenerating units are bounded by connective tissues forming the endoneurial tubules, having outer diameters similar to those of undamaged large myelinated fibers. Distal sections of nerve compressed at high pressure demonstrated extensive regeneration consistent with a prior Sunderland grade V injury, as evidenced by the complete replacement of normal caliber myelinated axons in the distal segment presence with regenerating units. Quantitative nerve histomorphometry demonstrated minimal change in myelinated axon caliber and counts between proximal and distal segments for nerve compressed at low pressure. At medium pressure, a moderate decrease in mean myelinated nerve caliber and increase in axon count was noted in distal sections as compared to proximal sections, consistent with

Grade III Sunderland injury. At high pressure, a larger decrease in mean myelinated axon caliber and larger increase in axon counts was observed for lesional and distal as compared to proximal sections, consistent with neurotmesis and subsequent spontaneous nerve regeneration across the gap.

4. Discussion

4.1. Summary

Described is the design, manufacture, and *ex vivo* and *in vivo* validation of a miniaturized, wireless, implantable device for study of entrapment neuropathy in a murine model. This approach is the first to enable titration and continuous monitoring of applied pressure to a peripheral nerve over the long term. Use of this device may be paired with functional assessments to correlate the degree and duration of nerve compression with nerve function in a variety of animal models. Herein, the device was employed to induce entrapment neuropathy of facial nerve branches controlling whisking function in the rat. Functional loss induced in this model spanned mild neurapraxia to
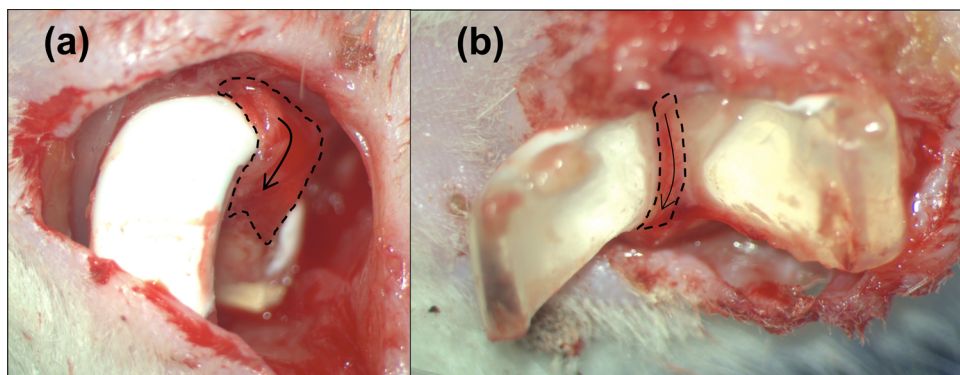

Fig. 7. Gross appearance of facial nerve branches at time of device explant. (a) In nerve compressed at low pressure (under 100 mmHg), normal appearing nerve is demonstrated. (b) Upon cuff release, nerve compressed at medium pressure (200 mmHg – 300 mmHg) demonstrates thinning and partial clarification (nerve borders identified by dashed lines, arrows delineate proximal to distal course.
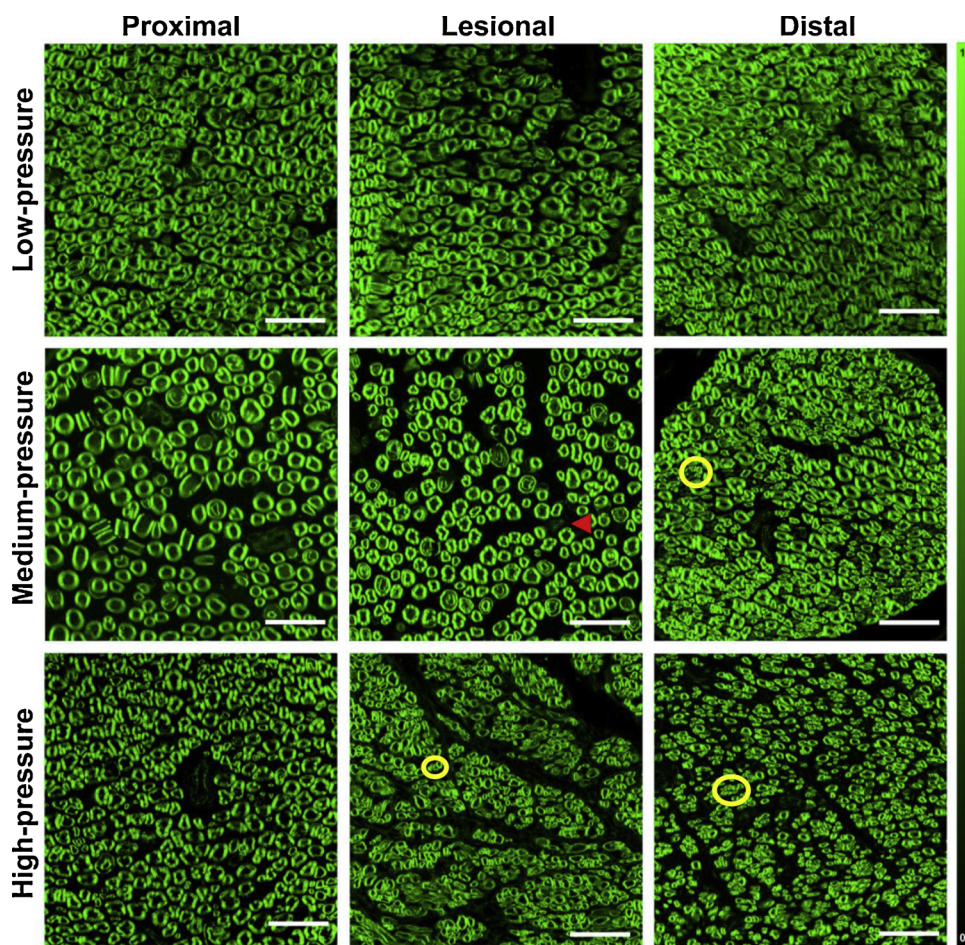
Fig. 8. Fluorescence imaging (above) of myelinated axons in cross-sections of facial nerve branches harvested several weeks after compression at low, medium, and high-pressures, and corresponding histomorphometry (below). Following compression at low pressure (under 100 mmHg), myelinated axons in proximal, lesional, and distal segments appeared similar. Nerve branches compressed between 200 mmHg and 300 mmHg demonstrated occasional Wallerian degeneration (arrowhead) in the area of compression, and several regenerating units (yellow circles) in the distal segment. Nerve previously compressed at high pressure (300 mmHg–500 mmHg) demonstrated extensive regenerating units (yellow circles) in the lesional and distal segments (Scale bar: 30 μm, Color bar: normalized intensity value (0–1). FluoroMyelin Green®, 1 μm sections, 63X).
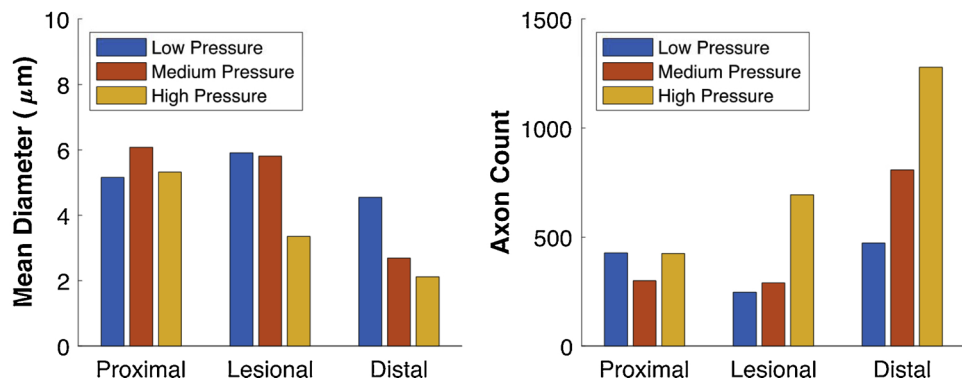
complete paralysis, demonstrating the utility of this approach to model a broad range of neural entrapment severity. This device could be employed to study the long-term effects of extrinsic compression and subsequent decompression of other accessible nerves in small animals. This approach provides opportunity to investigate the mechanics of entrapment neuropathy in greater depth than previously possible, carrying potential to enhance understanding and management of this devastating disease spectrum.

4.2. Limitations

Though the device and rodent model employed herein offers a cost-effective means for controlled study of entrapment neuropathy, caution is warranted with clinical translation of future research findings. Nerve entrapment syndromes may involve additional pathophysiologic mechanisms beyond the simple mechanical compression modeled herein,

including altered local microvascular environment or viral reactivation (Smith, 2014; Arnold and Elsheikh, 2013; Rempel et al., 1999; Rempel and Diao, 2004; Pham and Gupta, 2009; Wasiu Wahab et al., 2017). Further, rodents are known to undergo Wallerian degeneration at rates at least two-fold higher than humans, while exhibiting exceptionally robust neural regeneration (Gaudet et al., 2011; Coleman and Freeman, 2010). Nevertheless, we believe this model is likely to yield important insights into the role and timing of surgical decompression of peripheral nerves.

This model requires placement of a silicone cuff around a peripheral nerve. Neural dysfunction might occur in the absence of fluid injection into the hydraulic system via foreign body response, iatrogenic nerve injury at time of device implantation, or delayed traction injury during long-term implantation. Though capsule formation around the devices occurred in all animals, minimal capsule growth into the lumen of the occlusion cuff was noted after several days of implantation.

Neuropraxic injury was avoided with use of meticulous surgical technique at time of device implantation, and traction injury was avoided by securing of the occlusion cuffs to the underlying masseter muscle using surgical suture. Though device extrusion may occur, it was not observed in this series of animals.

4.3. Future directions

Though modelling of entrapment neuropathy of small peripheral nerves (1–2 mm diameter) in a rodent model has been demonstrated herein, this device could be fitted with a larger cuff for characterizing entrapment of larger nerves in higher order mammals. This device and its microcontroller backbone may be repurposed for cost-effective *in vivo* study of a wide range of disease processes. By placing the cuff around a vessel as opposed to a nerve, this device could even be employed for study of a variety of ischemic or vaso-occlusive disorders, including cerebrovascular accidents, hemodynamic shock, and free flap thrombosis. By virtue of its wireless transmission capabilities and open-source design, this device could be readily redesigned with alternative sensors for monitoring of other physiologic signals. For example, the pressure transducer and hydraulic system could be replaced with a pH sensor for continuous monitoring of acid-base shifts in tissues, or with an accelerometer for monitoring of gait and vestibular function. Device lifespan can be additionally extended via incorporation of components enabling wireless power transfer. Depending on the application, device power consumption could be optimized by adjusting the sampling rate of data acquisition and transmission.

Though a murine model of BP has been previously characterized (Sugita et al., 1995), no controlled animal model has been developed to characterize the impact of facial nerve decompression surgery. Future work will employ the approach described herein to characterize long-term facial functional recovery following facial nerve compression at various pressure levels and durations in a small animal model.

Declaration of Competing Interest

None.

Acknowledgements

Appendix A. Supplementary data

Supplementary material related to this article can be found, in the online version, at doi:https://doi.org/10.1016/j.jneumeth.2019.108461.

References

Adelaar, R.S., Foster, W.C., McDowell, C., 1984. The treatment of the cubital tunnel syndrome. J. Hand Surg. 9 (1), 90–95. https://doi.org/10.1016/S0363-5023(84)80193-8. 1984/01/01/.

Aguayo, A., Cherunada, P.V.N., Midgley, R., 1971. Experimental compression neuropathy in the rabbit; histologic and electrophysiologic studies. Arch. Neurol. 24.

Arnold, W.D.E., Elsheikh, B.H., 2013. Entrapment neuropathies. Neurol. Clin. 31 (2), 405–424.

Barac, S., Jiga, L.P., Barac, B., Honioiu, T., Dellon, A.L., Ionac, M., 2013. Hindpaw withdrawal from a painful thermal stimulus after sciatic nerve compression and decompression in the diabetic rat. J. Reconstr. Microsurg. 29 (1), 63–66.

Baugh, R.F., et al., 2013. Clinical practice guideline: Bell's Palsy (in eng). Otolaryngol.

Head. Neck Surg. 149 (3 Suppl), S1–27. https://doi.org/10.1177/0194599813505967.

Bodenez, C., Bernat, I., Willer, J.C., Barre, P., Lamas, G., Tankere, F., 2010. Facial nerve decompression for idiopathic Bell's palsy: report of 13 cases and literature review (in English). J. Laryngol. Otol. Rev. 124 (3), 272–278. https://doi.org/10.1017/S0022215109991265.

Cannon, R.B., Gurgel, R.K., Warren, F.M., Shelton, C., 2015. Facial nerve outcomes after middle fossa decompression for Bell's palsy (in English). Otol. Neurotol. 36 (3), 513–518. https://doi.org/10.1097/MAO.0000000000000513.

Chao, T., Pham, K., Steward, O., Gupta, R., 2008. Chronic nerve compression injury induces a phenotypic switch of neurons within the dorsal root ganglia. J. Comp. Neurol. 506 (2), 180–193. https://doi.org/10.1002/cne.21537.

Cheung, P.W.H., Hu, Y., Cheung, J.P.Y., 2019. Novel compression rat model for developmental spinal stenosis. J. Orthop. Res. 37 (5), 1090–1100. https://doi.org/10.1002/jor.24221.

Coleman, M.P., Freeman, M.R., 2010. Wallerian degeneration, wld(s), and nmnat. Annu. Rev. Neurosci. 33, 245–267. https://doi.org/10.1146/annurev-neuro-060909-153248.

Dahlin, L.B., McLean, W.G., 1986. Effects of graded experimental compression on slow and fast axonal transport in rabbit vagus nerve. J. Neurol. Sci. 72 (1), 19–30.

de Ruiter, G.C.W., et al., 2008. Misdirection of regenerating motor axons after nerve injury and repair in the rat sciatic nerve model (in eng). Exp. Neurol. 211 (2), 339–350. https://doi.org/10.1016/j.expneurol.2007.12.023.

Dellon, A.L., Mackinnon, S., 1991. Chronic nerve compression model for the double crush hypothesis. Ann. Plast. Surg. 26 (3), 259–264.

Dyck, P.J., Lais, A.C., Giannini, C., Engelstad, J.K., 1990. Structural alterations of nerve during cuff compression. Neurobiology 87, 9828–9832.

Fisch, U., 1981. Surgery for Bell's Palsy. Arch Otolaryngol 107.

Fisch, U., Esslen, E., 1972. Total intratemporal exposure of the facial nerve. Pathologic findings in Bell's palsy. Arch Otolaryngol 95 (4), 335–341.

Gantz, B.J., Rubinstein, J.T., Gidley, P., Woodworth, G.G., 1999. Surgical management of Bell's Palsy. Laryngoscope 109.

Gaudet, A.D., Popovich, P.G., Ramer, M.S., 2011. Wallerian degeneration: gaining perspective on inflammatory events after peripheral injury. J. Neuroinflammation 8 (1), 1.

Gilden, D.H., 2004. Clinical practice: Bell's Palsy. N. Engl. J. Med. 351, 1323–1331.

Gupta, R., Rowshan, K., Chao, T., Mozaffar, T., Steward, O., 2004. Chronic nerve compression induces local demyelination and remyelination in a rat model of carpal tunnel syndrome. Exp. Neurol. 187 (2), 500–508.

Hato, N., et al., 2012. Facial nerve decompression surgery using bFGF-impregnated biodegradable gelatin hydrogel in patients with Bell palsy. Otolaryngol. - Head Neck Surg. 146 (4), 641–646. https://doi.org/10.1177/0194599811431661.

Hazama, H., Tamaki, H., Nomura, A., Furukawa, Y., Uetsuka, H., 1972. Compression of the facial nerve. Arch. Otolaryngol. 95 (4), 346–349.

Heaton, J.T., Kowaleski, J.M., Bermejo, R., Zeigler, H.P., Ahlgren, D.J., Hadlock, T.A., 2008. A system for studying facial nerve function in rats through simultaneous bilateral monitoring of eyelid and whisker movements. J. Neurosci. Methods 171 (2), 197–206. https://doi.org/10.1016/j.jneumeth.2008.02.023.

Latinovic, R., Gulliford, M.C., Hughes, R.A.C., 2006a. Incidence of common compressive neuropathies in primary care (in eng). J. Neurol. Neurosurg. Psychiatr. 77 (2), 263–265. https://doi.org/10.1136/jnnp.2005.066696.

Latinovic, R., Gulliford, M.C., Hughes, R.A.C., 2006b. Incidence of common compressive neuropathies in primary care. J. Neurol. Neurosurg. Psychiatr. 77, 263–265.

Liu, S., et al., 2013. Study on relationship between operation timing and clinical prognosis of cases with Bell palsy. J. Clin. Otorhinolaryngol. Head Neck Surg. 27 (13), 698–700.

Liu, Z., Chen, Z., Chen, J., 2018. A novel chronic nerve compresion model in the rat. Neural Regen. Res. 13 (8), 1477–1485.

Mackinnon, S., Dellon, A.L., Hudson, A.R., Hunter, D.A., 1985. A primate model for chronic nerve compression. J. Reconstr. Microsurg. 1 (3), 185–195.

Mohan, S., et al., 2018. Fluorescent reporter mice for nerve guidance conduit assessment: a high-throughput in vivo model. Laryngoscope 128 (11), E386–E392. https://doi.org/10.1002/lary.27439.

Montserrat, L., Benito, M., 1988. Facial synkinesis and aberrant regeneration of facial nerve (in eng). Adv. Neurol. 49, 211–224.

Morris, J.H., Hudson, A.R., Weddell, G., 1972. A study of degeneration and regeneration in the divided rat sciatic nerve based on electron microscopy. II. The development of the "regenerating unit. Zeitschrift fur Zellforschung und mikroskopische Anatomie 124 (1), 103–130.

Murakami, S., Mizobuchi, M., Nakashiro, Y., Doi, T., Hato, N., Yanagihara, N., 1996. Bell palsy and herpes simplex virus: identification of viral DNA in endoneurial fluid and muscle (in English). Annals of Internal Medicine, Research Support, Non-U.S. Gov't 124 (1 Pt 1), 27–30.

O'Brien, J.P., Mackinnon, S., MacLean, A.R., Hudson, A.R., Dellon, A.L., Hunter, D.A., 1987. A model of chronic nerve compression in the rat. Ann. Plast. Surg. 19 (5), 430–435.

Phalen, G.S., Kendrick, J.I., 1957. Compression neuropathy of the median nerve in the carpal tunnel. JAMA 164 (5), 524–530. https://doi.org/10.1001/jama.1957.02980050014005.

Pham, K., Gupta, R., 2009. Understanding the mechanisms of entrapment neuropathies. Neurosurg. Focus 26 (2). https://doi.org/10.3171/FOC.2009.26.2.E7.

Rempel, D.M., Diao, E., 2004. Entrapment neuropathies: pathophysiology and pathogenesis. J. Electromyogr. Kinesiol. 14 (1), 71–75. https://doi.org/10.1016/j.jelekin.2003.09.009.

Rempel, D.M., Dahlin, L., Lundborg, G., 1999. Pathophysiology of nerve compression syndromes: response of peripheral nerves to loading. J. Bone Jt. Surg. 81–A (11).

Schindelin, J., et al., 2012. Fiji: an open-source platform for biological-image analysis (in

Eng). Nat. Methods 9 (7), 676–682. https://doi.org/10.1038/nmeth.2019.

Schneider, C.A., Rasband, W.S., Eliceiri, K.W., 2012. NIH Image to ImageJ: 25 years of image analysis. Nat. Methods 9 (7), 671–675.

Shapira, Y., Migirov, L., Kronenberg, J., 2006. Facial nerve decompression. Harefuah 145 (8), 557–560 632.

Smith, B.E., 2014. Focal and entrapment neuropathies. Handbook of Clinical Neurology; Diabetes and the Nervous System 126 no. 3, ch. 3.

Smouha, E., Toh, E., Schaitkin, B.M., 2011. Surgical treatment of Bell's palsy: current attitudes (in English). Laryngoscope 121 (9), 1965–1970. https://doi.org/10.1002/lary.21906.

Sugita, T., Fujiwara, Y., Murakami, S., Hirata, Y., Yanagihara, N., Kurata, T., 1995. Facial nerve paralysis induced by herpes simplex virus in mice: an animal model of acute and transient facial paralysis. Ann. Otol. Rhinol. Laryngol. 104 (7), 574–581.

Sumner, A.J., 1990. Aberrant reinnervation. Muscle Nerve 13 (9), 801–803. https://doi.org/10.1002/mus.880130905.

Sunderland, S., 1951. A classification of peripheral nerve injuries producing loss of function. Brain 74 (4), 491–516. https://doi.org/10.1093/brain/74.4.491.

Teasdall, R.D., Salman, S.D., 1971. Mass facial movements: electromyographic evidence for misdirection (in eng). Neurology 21 (6), 652–654. https://doi.org/10.1212/wnl.21.6.652.

Valls-Sole, J., Tolosa, E.S., Pujol, M., 1992. Myokymic discharges and enhanced facial nerve reflex responses after recovery from idiopathic facial palsy (in eng). Muscle Nerve 15 (1), 37–42. https://doi.org/10.1002/mus.880150107.

Wang, W., Kang, S., Coto Hernandez, I., Jowett, N., 2019. A rapid protocol for intraoperative assessment of peripheral nerve myelinated axon count and its application to cross-facial nerve grafting. Plast. Reconstr. Surg. 143 (3), 771–778. https://doi.org/10.1097/PRS.0000000000005338.

Wasiu Wahab, K., Sanya, E.O., Adebayo, P.B., Babalola, M.O., Ibraheem, H.G., 2017. Carpal tunnel syndrome and other entrapment neuropathies. Oman Med. J. 32 (6), 449–454.

Weber, E.D., Newman, S.A., 2007. Aberrant regeneration of the oculomotor nerve: implications for neurosurgeons (in eng). Neurosurg. Focus 23 (5), E14. https://doi.org/10.3171/foc-07/11/e14.

Wu, S.H., Chen, X., Wang, J., Liu, H., Qian, X.Z., Pan, X.L., 2015. Subtotal facial nerve decompression in preventing further recurrence and promoting facial nerve recovery of severe idiopathic recurrent facial palsy (in English). Eur. Arch. Oto-Rhino-Laryngol. 272 (11), 3295–3298. https://doi.org/10.1007/s00405-014-2991-9.